JMEPEG (2012) 21:1395–1404
DOI: 10.1007/s11665-011-0019-9

1059-9495/$19.00

Influence of Elevated Temperature and Stress Ratio on the Fatigue Response of AM60B Magnesium Alloy

Md. Nur-Hossain and Farid Taheri

(Submitted May 3, 2011; in revised form June 23, 2011)

The fatigue response of a high pressure die-cast AM60B Mg alloy is studied at room and elevated temperatures. The fatigue tests are conducted with stress ratio of $R = 0.1$ and frequency of 30 Hz. The main objective is to determine whether elevated temperature would affect the fatigue response of the alloy. In addition, fatigue crack growth characteristics of the alloy is investigated at room temperature. The purpose of this test is to ascertain the capability and accuracy of a finite element approach coupled with the Walker model in assessing the life cycle of the alloy, in consideration of the influence of stress ratio.

Keywords AM60B magnesium alloy, fatigue crack growth rate, finite element method, linear elastic fracture mechanics, scanning electron microscope, single edge notch tension

1. Introduction

Magnesium alloys are increasingly being used in the automobile and light truck industries. Among all other magnesium alloys, cast magnesium alloys are finding incremental use in the automotive industry due to their high-specific strength, lower density and excellent castability and machinability in comparison to the commonly used metallic materials. As a result, ongoing interest in the use of cast magnesium alloys in the automotive industry has recently triggered substantial research efforts to be focused on characterization of the structural properties of the metals (Ref 1). The increased use of the alloy in various fields demands knowledge about the fatigue properties and fracture response of the alloy. Therefore, before utilization of magnesium alloys in structural applications, the determination of their fatigue lives and crack propagation characteristics at different stress ratios is necessary. Moreover, depending on the application, the environment might play a vital role on the fatigue life cycle of these alloys, since it is well-established that metals fatigue life cycles are markedly affected by changes in their environment (Ref 2).

Assessment of fatigue performance, at room or elevated temperatures, is an integral part of the life assessment of any component, especially those employed in automobiles. As the uses of cast magnesium alloys is gaining higher demand in structural and high-temperature applications, the understanding of fatigue response of such cast alloys at elevated temperature becomes more imperative.

In this study, AM60B magnesium alloy, which has been characterized as an alloy with outstanding ductility and energy absorbing properties, combined with good strength, light weight, and castability, is considered. Materials, especially those with relatively low fracture toughness, might fail even below their ultimate strength. The failure can be analyzed on the basis of linear elasticity concepts, through the use of the linear elastic fracture mechanics (LEFM) (Ref 3). High strength, light weight metallic alloys, such as those used in aerospace industry, are examples of such materials (Ref 3). By using LEFM, it is possible to make a direct comparison of fatigue crack growth behavior of the engineering components or structures and their counterpart laboratory specimens, using the stress intensity factor (SIF) range, ΔK (Ref 4).

In recent years, some research works have been carried out on characterizing the fatigue response of various die-cast magnesium alloys (Ref 1, 5). However, the work on high pressure die-cast (HPDC) magnesium alloys has been quite limited. Koch (Ref 6) investigated the fatigue limit of HPDC AM60 magnesium alloy. Later, Lu et al. (Ref 7, 8) reported the fatigue characterization of HPDC AM60B magnesium alloy at room temperature. However, the above authors did not investigate the fatigue response of the alloy at elevated temperature.

Nomenclature

C_P	Paris model constant
da/dN	Crack growth rate
K	Stress intensity factor
ΔK	Stress intensity factor range
ΔK_{eq}	Effective stress intensity factor range
m_p	Paris model exponent
R	Stress ratio
γ	Material parameter
σ_y	Yield stress
α	Ratio between crack length and width of the specimen

Md. Nur-Hossain and **Farid Taheri**, Department of Civil and Resource Engineering, Dalhousie University, 1360 Barrington Street, Halifax, NS B3J 1Z1, Canada. Contact email: farid.taheri@dal.ca.

One of the few works investigating the influence of temperature on the fatigue of such alloys has been the work of Wang and Fan (Ref 1); they investigated the fatigue crack growth behavior of AM50 magnesium alloy at elevated temperature. They found that the growth rate of small fatigue cracks increased when temperature increased. Moreover, investigation into the influence of stress ratio on the fatigue response of these alloys is as scarce. One of the few notable works on this topic is that by Ishihara et al. (Ref 9), who explained that the influence of mean stress on the fatigue strength can be described approximately by the Gerber relationship as follows:

$$\sigma = \sigma_{(R=-1)}\left\{1 - \left(\frac{\sigma_m}{\sigma_{UTS}}\right)^2\right\} \quad \text{(Eq 1)}$$

where σ is the stress amplitude corresponding to the fatigue strength at a given mean stress σ_m; $\sigma_{(R=-1)}$ is the fatigue strength at $R = -1$, and σ_{UTS} is the ultimate tensile strength.

Zenga et al. (Ref 10) also observed that the loading ratio had a significant influence on the fatigue crack propagation rate of an extruded magnesium AZ80 alloy, and that it increased with an increase in load ratio.

2. Motivation and Synopsis of the Investigation

The lack of information on the influence of temperature and stress ratio on the fracture and fatigue response of HPDC AM60 magnesium alloy therefore motivated the work presented here. In this study, static tensile tests were performed on specimens extracted from thin die-cast AM60B magnesium alloy plates at room temperature condition, in order to characterize the alloy's basic mechanical properties. The response of the alloy was also studied under elevated temperature. The fatigue tests were conducted at a stress ratio of $R = 0.1$ at 30 Hz frequency, at both room and elevated temperatures. As well, fatigue crack growth rates (FCGRs) were recorded under the abovementioned conditions, and under different stress ratios. The objective was to determine the growth rate at various stress ratios under the same loading frequency, thereby examining the influence of the stress ratio on fatigue life and crack growth rate of the alloy. The analytical models used were first the Paris model, followed by the Walker model, in order to characterize the stress ratio's effect. LEFM analyses were conducted for different crack lengths. The assessments of the FCGR of AM60B magnesium alloy, using the abovementioned models, were carried out using the NISA/ENDURE (Ref 11, 12) finite element (FE) codes and fatigue analysis.

3. Material and Compositions

Most commercial Mg alloys contain 2-9 wt.% aluminum. Under equilibrium conditions, the cast Mg-alloy should solidify as a single phase α-Mg solid solution and further cooling should lead to the solid state precipitation of β-$Mg_{17}Al_{12}$ within the α-grains (Ref 1). The presence of the brittle eutectic phase $Mg_{17}Al_{12}$ affects mainly the mechanical properties of cast Mg alloys (Ref 13). For this study, test specimens were extracted from die-cast AM60B Mg alloy plates provided by the Meridian Technologies Inc. (Strathroy, Ontario). The chemical composition of the alloy is shown in Table 1.

Energy dispersive x-ray analysis (EDS) had also been done for the different phases of the AM60B magnesium alloy. The outcomes are shown in Table 2-4, along with the scanning electron microscopic (SEM) images shown in Fig. 1, which represent a general view of the microstructure of different phases of AM60B alloy. As seen, the weight percentage of the Al element in α-Mg phase is greater than the other phases.

4. Experimental Procedures

4.1 Specimens and Test Setup

Flat dog-bone shaped tensile and fatigue specimens were extracted from the plates according to ASTM standard E-8M (Ref 14) (Fig. 2a), and E-466 (Fig. 2b), respectively, for the static and cyclic tests (Ref 15). The dimensions of the specimens are also illustrated in the figures.

The specimens were prepared with proper surface finishing operation and the damaged metal on the machined surface was removed by grinding and polishing. The mechanical properties of the alloy were measured by uniaxial tensile test following ASTM E8.

The research included monotonic test, conducted at room temperature to evaluate the basic mechanical properties of the alloy. Furthermore, cyclic tests were conducted both at room

Table 2 EDS elements analysis of α-Mg phase

Alloy	C	O	Mg	Al	Total
Wt.%	4.21	12.67	72.49	10.63	100.00
At.%	7.77	17.53	65.99	8.72	100.00

Table 3 EDS elements analysis of β-phase

Alloy	C	O	Mg	Al	Total
Wt.%	2.32	6.10	68.76	22.83	100.00
At.%	4.54	8.97	66.57	19.92	100.00

Table 4 EDS elements analysis of Mn rich intermetallic phase

Alloy	C	O	Mg	Al	Si	Mn	Total
Wt.%	5.28	27.01	45.69	17.72	0.56	3.73	100.00
At.%	9.25	35.53	39.55	13.82	0.42	1.43	100.00

Table 1 Composition of cast AM60B magnesium alloy in wt.%

Alloy	Al	Mn	Si	Zn	Cu	Fe	Ni	Other	Mg
Cast AM60B	5.5-6.5	0.25 min	0.10 max	0.22 max	0.010 max	0.005 max	0.002 max	0.003 (total)	Bal.

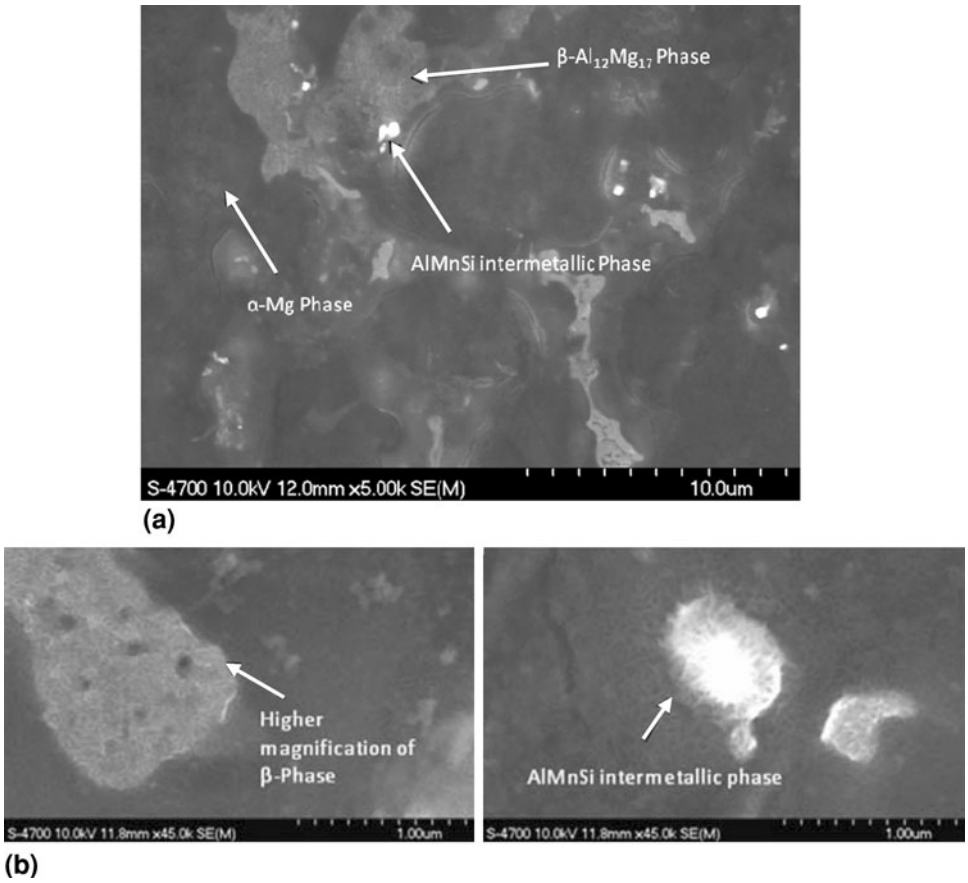

Fig. 1 (a) Different phases of AM60B magnesium alloy and (b) β-phase and Mg-rich intermetallic phase in higher magnification

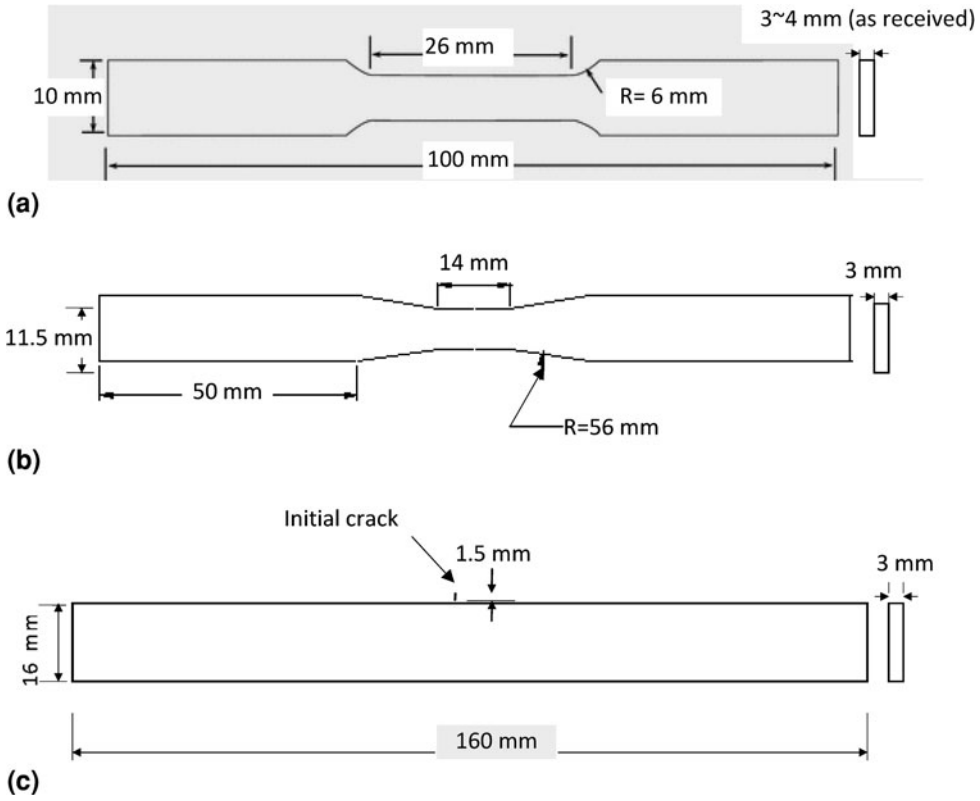

Fig. 2 (a) ASTM E8M tensile specimen, (b) E-466 fatigue specimen, and (c) ASTM E647 specimen (drawings not to scale)

and at elevated temperature of 80 °C in a servo-hydraulic Instron 8501 machine, using the Test Star control system (Instron, Norwood, MA). Finally, fatigue crack propagation investigation was conducted for specimens tested at room temperature only, since the measurement equipment could not be used within the environmental chamber at the elevated temperature.

For fatigue tests, five stress amplitudes were considered from 75 to 115 MPa with 10 MPa increments. Similar to the work of Wang and Fan (Ref 1), all fatigue tests were load controlled at a stress ratio $R = 0.1$. A standard extensometer (Instron, Norwood) was used to measure the strain within the gage length of the specimen tensile testing. A ZBD-104 environmental chamber, manufactured by the Associated Environmental System (Ayer, MA), was used for fatigue tests at elevated temperature. Both an optical microscope and a SEM (Hitachi) was used to examine pores and other possible crack initiation sites and microstructures.

4.2 Fatigue Crack Propagation Tests

The single edge crack flat specimen geometry was used for the fatigue crack growth tests. The specimens were prepared according to the ASTM E647 standard (Ref 16). The dimensions of the specimen are illustrated in Fig. 2(c). The specimen had an initial notch of 1-mm long, which was subsequently subject to a cyclic load to take the notch to a sharp crack, with a total length of 1.5 mm. The fatigue crack propagation cyclic test was conducted using the same test machine and control system. The tests were performed under load control at stress ratios $R = 0$, 0.1, and 0.2, with the maximum stress value of 80 MPa and frequency of 30 Hz. These stress ratios were selected in conformance to the intended use of the alloy in specific automotive applications, as well as accommodating testing with reasonable elapsed time periods. The incremental lengths of fatigue cracks were measured at approximately every 0.5 mm increment, directly through the use of a Mitutoyo traveling microscope with a magnification of 50×, mounted on a pair of micrometers with a resolution of 0.01 mm. The specimens were first notched by a jeweller's saw, and subsequently fatigue precracked to introduce a sharp initial crack for the actual fatigue crack growth test. Once the fatigue precrack was formed, extension of the growing crack was recorded as a function of crack length increment and the associated number of cycles. The recording was continued until the specimen had failed. The crack growth length (a) versus number of cycles (N) curve was plotted for each specimen, which was subsequently postprocessed to generate the da/dN versus ΔK curve (Ref 17).

5. Results and Discussion

5.1 Static (Monotonic) Tension Test Results

As stated earlier, the basic mechanical properties of the alloy were evaluated by conducting the tensile test at room temperature. Figure 3 shows the stress versus strain relationship of HPDC AM60B magnesium alloy generated from the tension test data conducted at room temperature. The average yield strength of the material was determined to be 145 MPa. The variation in the plastic region and ultimate tensile strength is due to the large variation in porosity in the cast alloy, as

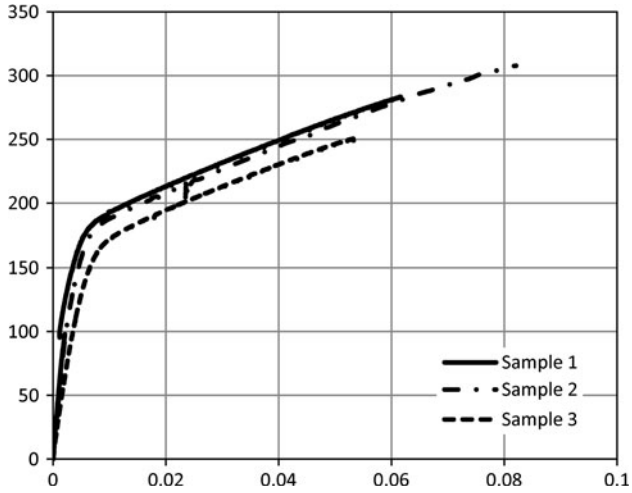

Fig. 3 Tensile stress-strain curve for HPDC AM60B magnesium alloy

observed through the optical and SEM images. The average elongation at fracture was found approximately 6.6%. True stress and true strain were subsequently evaluated by using the standard mechanics of materials equations (Ref 18).

5.2 Fatigue Test Results

5.2.1 Influence of the Elevated Temperature on Fatigue Response of AM60B Magnesium Alloy. The results of cyclic tests conducted at room and elevated temperature are illustrated in Fig. 4. A run-out cycle limit of 10^6 at stress level 75 MPa was determined for all specimens tested at the two temperatures. The fatigue test was continued up to complete failure of the specimen, while the test was stopped when the specimen did not fail up to 10^6 cycles. Results indicated that there was no significant difference in the number of cycles to failure between room and elevated temperatures at a stress level of 85 MPa, as is illustrated in the respective S-N curves in Fig. 4. It can be seen that at the so-called run-out (relatively lower) stress level, the effect of the elevated temperature (i.e., 80 °C) on fatigue life of AM60B magnesium alloy is not significant.

As stated, the tests were conducted at five stress levels, both at room and elevated temperature. The failed specimens underwent micrograph and microscopic examinations with the objective of observing any significant changes to the fracture surfaces due to the variation in the test environment (i.e., from room to the elevated temperatures). The representative images have been shown in Fig. 5. The images represent the condition of the alloy having been subjected to cyclic loading at both room and elevated temperatures. The images show the cross section of the specimens at a location just underneath the fracture surface (after the surface was polished). The influence of the elevated temperature was observed to be more significant when the alloy was subject to higher stress levels. Segregation of the β-Mg was observed to occur in the vicinity of the pores' boundary at the elevated temperature. The interaction between two adjacent pores leading to creation of a cavity was also observed for the specimens tested at elevated temperature. Moreover, the pores were noted to expand in the specimens tested under the elevated temperature.

Furthermore, examination of the results illustrated in Fig. 4 indicates that there appears to be a threshold stress at which

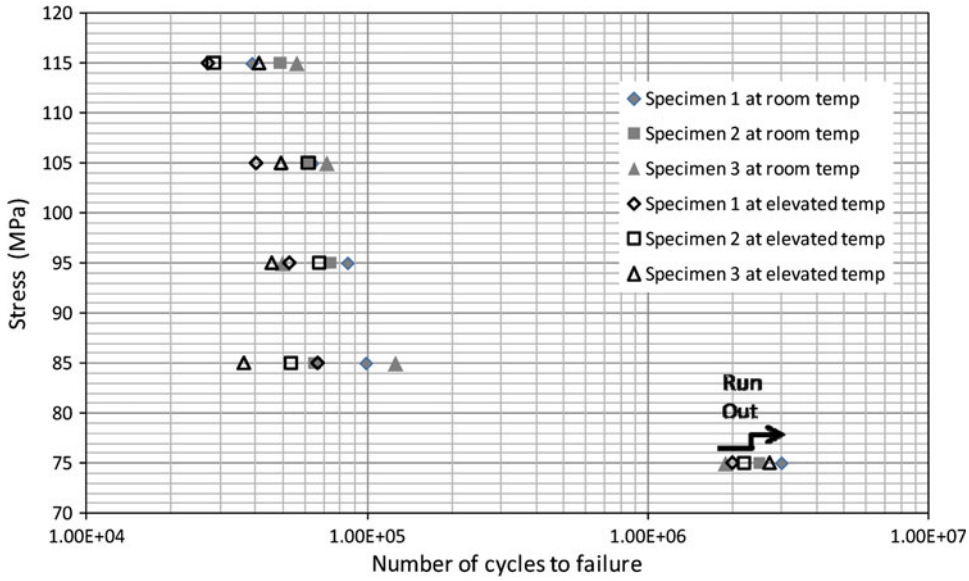

Fig. 4 S-N curves for AM60B at room and elevated temperature (800 °C)

(and presumably, below which), the effect of temperature on the fatigue life in this alloy subsides. One may also conclude from the results that for the stress values at and above 85 MPa, the effect of temperature on the fatigue life is more or less similar (and in fact in average it is a bit more significant for the case of specimens tested under 85 MPa stress).

Fractography analysis was conducted to further characterize the fracture behavior of die-cast AM60B magnesium alloy. As seen in Fig. 5, it can be identified that the expansion of pores creates microcracks, thus facilitating the subsequent crack propagation. The small fatigue crack growth path at the elevated temperature is different from that at room temperature. At elevated temperature, huge segregation of β-$Mg_{17}Al_{12}$ occurs in the vicinity of the pore's boundary; this is believed to be due to the change in brittle nature of the hard β-$Mg_{17}Al_{12}$. Moreover, the interaction between two adjacent pores for creating a cavity is more significant, as identified for specimens tested at the elevated temperature (see Fig. 5b and c). In contrast, at room temperature, even at high-stress level, no such segregation of β-$Mg_{17}Al_{12}$ could be observed.

The crack tip SIF is lower at lower stress levels; as a result the lower driving force, created at the crack tip, cannot cleave the microstructure. Indeed, at lower stress and elevated temperature, microcracks propagate with repeated sharpening and blunting; and as a result, no cleavage fracture occurs. Comparison of the pore boundary, shown in Fig. 5(a) (for specimens tested at room temperature), and that tested at elevated temperature (Fig. 5b and c), illustrates that β-$Mg_{17}Al_{12}$ segregation occurs at the elevated temperature (evident by the white spots visible around the pore in Fig. 5c). However, at high-stress level, the growth behavior of these small fatigue cracks indicates that many α-Mg grains were cleaved along the crack growth path at the elevated temperature, regardless of the stress level; this can be observed through the SEM images shown in Fig. 6(a), with a more magnified display of the region shown in Fig. 6(b). The main reason for this behavior is postulated to be due to the variation in the brittleness of the β particles at the elevated temperature. Therefore, the FCGR of a small crack would be faster at elevated temperature than that at room temperature. Consequently, the fatigue life at the elevated temperature is shorter than that at room temperature, as supported by the experimental results.

Another important issue is the presence of the foreign particles. These particles are complex compounds of the alloying elements, like Si and Cu. These particles are used to improve the castability and machinability. First, the large particles are released or break; as a result creating widely spaced holes close to the crack tip. In the final phase, pores are formed within myriads of smaller particles. Subsequently, these pores gradually coalesce to complete the fracture as shown in Fig. 7. Commencement of the small fatigue cracks occur along the interfaces of α-Mg grains, due to plastic slipping of surface grains.

6. Influence of the Stress Ratio on Fatigue Characterization of AM60B Magnesium Alloy

6.1 Analytical Prediction

FCGR can be easily evaluated as a function of SIF range. One of the popular methods to design and analysis fatigue growth rate is the Paris model. The simplest ways to determine the fatigue growth rate by using the Paris model, mathematically represented by

$$\frac{da}{dN} = C_P(\Delta K)^{m_p} \quad \text{(Eq 2)}$$

In the above equation, C_P is the Paris constant, $\frac{da}{dN}$ is the FCGR, ΔK indicates the SIF range, and m_p is the Paris exponent.

The Paris model was subsequently extended by Walker (Ref 19) for estimating the fatigue crack propagation life by accounting for the stress ratio, R. According to the Walker model, crack propagation rate can be related to the equivalent range of SIF, ΔK_{eq} using the following relationship:

$$\frac{da}{dN} = C_P(\Delta K_{eq})^{m_p} \quad \text{(Eq 3)}$$

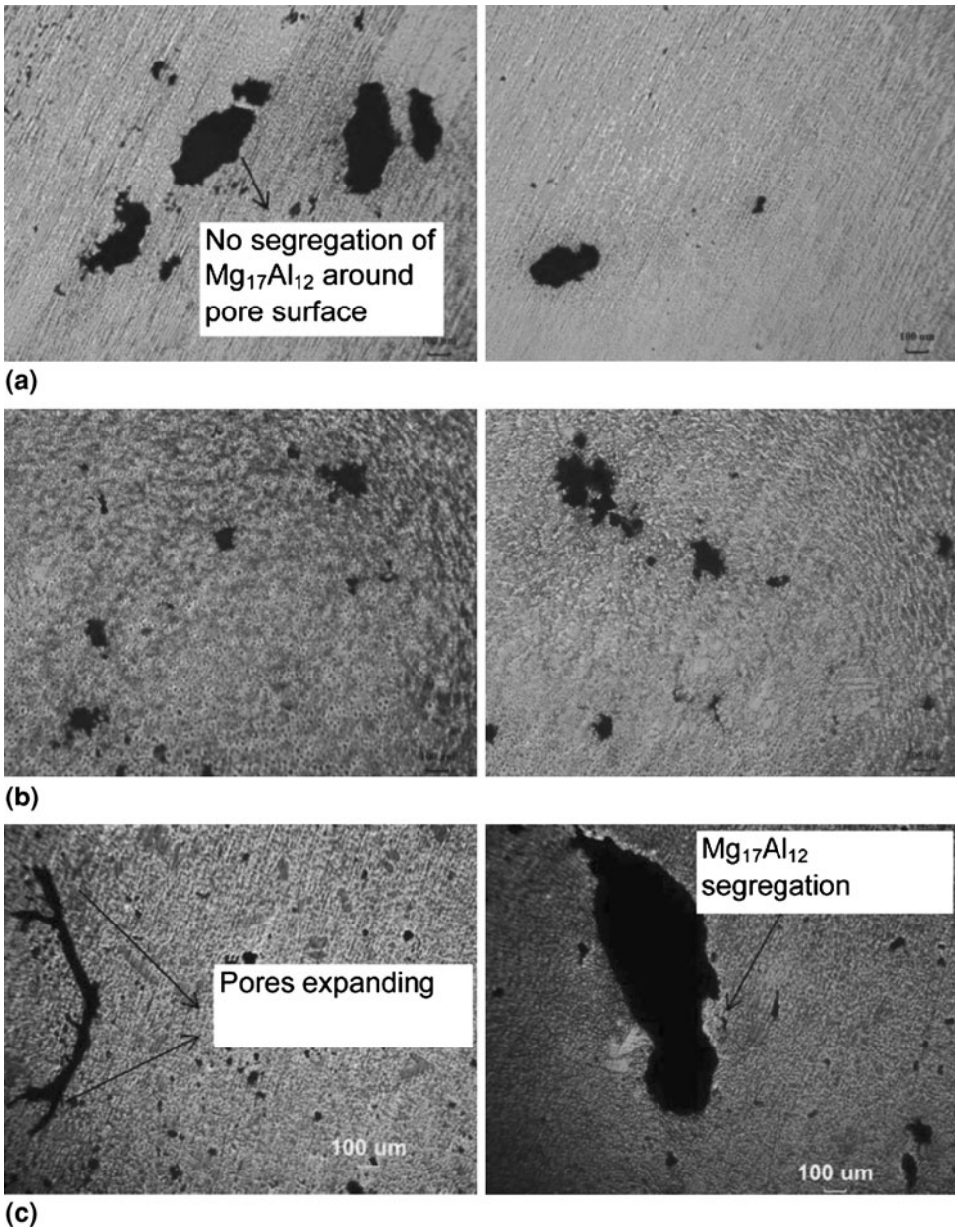

Fig. 5 Micrograph of fatigue specimen (a) at high-stress level (95-115 MPa) at room temperature, (b) at low-stress level (75-85 MPa) at elevated temperature, and (c) at high-stress level (95-115 MPa) at elevated temperature

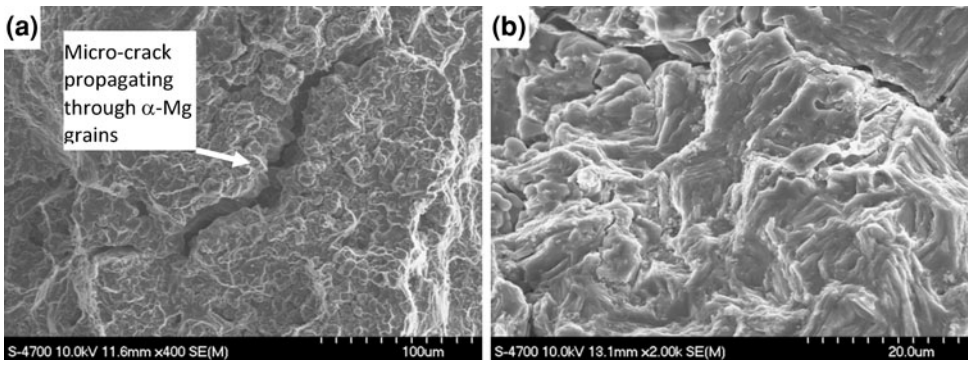

Fig. 6 SEM images showing crack passing through α-Mg at elevated temperature

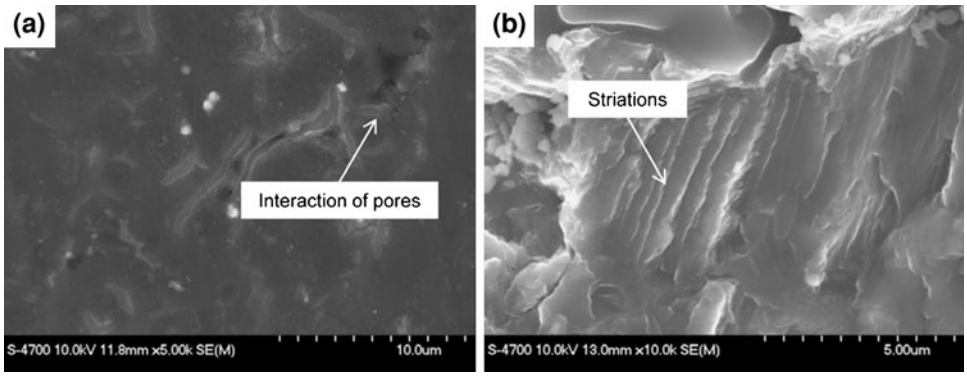

Fig. 7 SEM image showing (a) interaction of pores and inclusion particles. (b) Striations due to consecutive sharpening and blunting of micro-cracks

where

$$\Delta K_{\text{eq}} = \frac{\Delta K}{(1-R)^{1-\gamma}} \quad \text{(Eq 4)}$$

in which

$$\Delta K = Y \Delta\sigma \sqrt{\pi a_{\text{avg}}} \quad \text{(Eq 5)}$$

and

$$\left[Y = 0.265(1-\alpha)^4 + \frac{0.857 + 0.265\alpha}{(1-\alpha)^{3/2}} \right] \quad \text{(Eq 6)}$$

In the above equations, Y is the geometric factor, α is the ratio between crack length to width, and γ is a material parameter ranging from 0.3 to 0.8 (Ref 4, 20) and (Ref 21).

It is well-established that for a given initial crack size, the fatigue life would be a function of the magnitude of the applied stress and the fracture resistance of the material (Ref 19). The procedure therefore entails the evaluation of the SIF range, ΔK, for a given crack growth rate da/dN. The Walker model has been widely used in the aerospace industry (Ref 20), because it is simple to apply, requires only one additional parameter (γ, which is usually assumed to be 0.5), and produces reasonable results for many materials, provided that R is not too high.

As stated earlier, at positive stress ratios, the exponent γ usually takes values between 0.3 and 0.8. When, $\gamma = 0.3$, there would be a strong dependency of FCP to R, while $\gamma = 0.8$ produces a weaker dependence on R (Ref 1). The exact value of γ is not known for AM60B magnesium alloy at stress ratio of $R = 0.1$; usually $\gamma = 0.5$ is assumed, which is known to produce a reasonable estimate (Ref 1, 22).

Figure 8 shows the FCGR as a function of SIF range under different stress ratios (i.e., $R = 0$, 0.1, 0.2) of AM60B magnesium alloy at room temperature. Moreover, the ability of Walker's model in predicting the fatigue crack ratio, especially under the influence of stress ratio is illustrated in Fig. 9. In this figure, the experimental results are shown by solid lines (thinner lines for $R = 0.1$ and thicker lines for $R = 0.2$). The predictions of Walker's model are illustrated by dashed lines (again, thinner lines for $R = 0.1$ and thicker lines for $R = 0.2$). The analytical FCGRs plotted in Fig. 9 were calculated based on modification of the data for the case of no stress ration ($R = 0$), using Walker's model, with the parameters noted above. The results clearly show that the crack growth rate is dependent on the stress ratio and this effect would be stronger

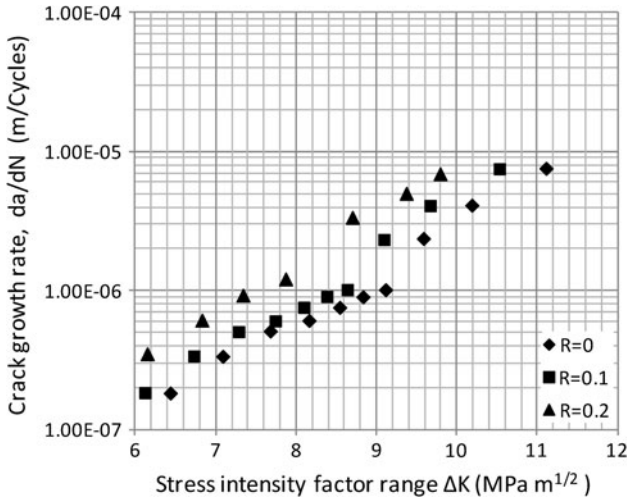

Fig. 8 Fatigue crack growth rate as a function of stress intensity factor range under different stress ratio of AM60B at room temperature

at a larger stress ratio. In all, the results obtained analytically compare favorably to the experimental results; the small differences between the experimental and analytical results are mainly due to the nonuniformity in porosity distribution within the specimens. As can be seen, the influence of porosity distribution becomes more pronounced at higher crack growth rates. As can also be seen, the FCG rate increases as a function of the stress ratio.

6.2 Finite Element Prediction

As stated above, a further FE investigation was conducted to assess the FCGR of AM60B magnesium alloy. The analysis was conducted using the FE code NISA (Ref 11), followed by postprocessing of the results (SIFs) obtained through the FE analysis by NISA's Endure fatigue crack propagation analysis module (Ref 12).

The specimen (shown in Fig. 2c) was modeled using nearly 6374 eight-node plane stress elements (NKTP 1) of NISA. The crack tip singularity was simulated by the "quarter-point" technique (Ref 11). A mesh convergence study was also conducted to ensure accurate evaluation of the crack tip SIF.

In NISA, the SIF is calculated using several techniques; we used the virtual crack closure technique (VCCT). In the VCCT, the strain energy release rate is computed through calculation of

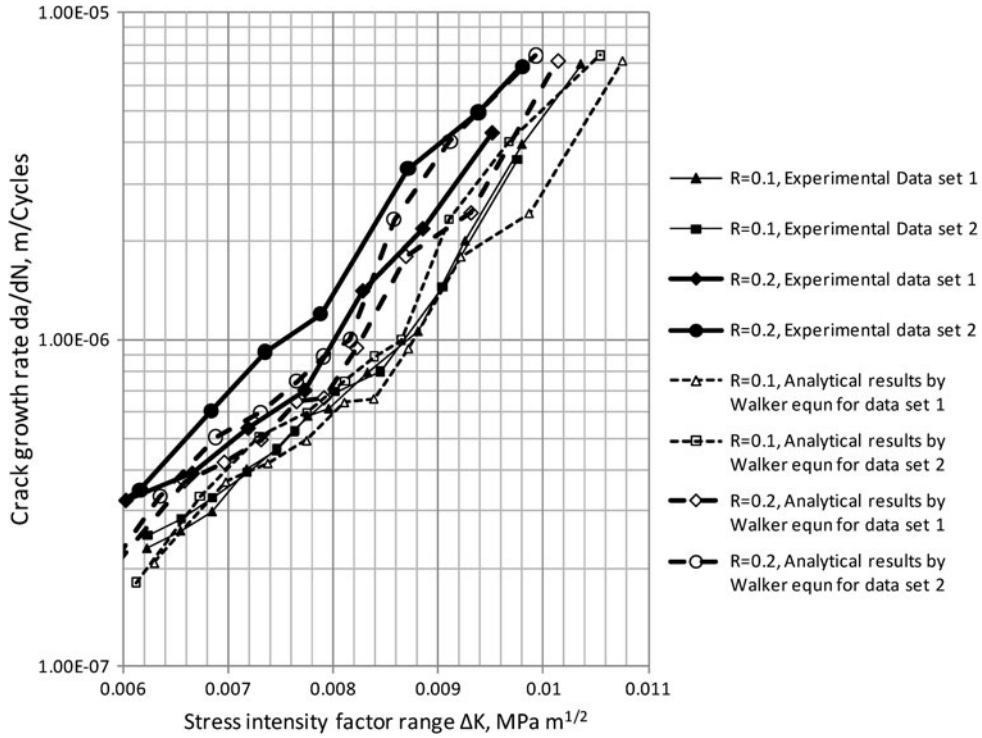

Fig. 9 Comparison of fatigue crack growth rates calculated by the Walker model and the experimental data

the crack tip neighboring nodal forces and displacements (the nodes on the cracked ligaments, neighboring the crack tip nodes), from which the stress intensity is subsequently calculated using the conventional LEFM relationship (Ref 17). From the FE perspective, VCCT is an effective and widely used method for evaluating the SIF, because it is not very sensitive to the FE mesh size. As a result, accurate results can be obtained, even with using relatively coarse meshes for modeling the crack tip. Due to this reason, VCCT is relatively easy to apply, eliminating the extra effort required for mesh refinement demanded by the other relevant techniques. As a result, VCCT is implemented into several FE software packages, like the GENOA/PFA, ABAQUS, NISA/ENDURE, and other progressive failure analysis tools (Ref 17).

As stated, the FCGR analysis is conducted in the Endure environment of the NISA. Once the stress intensity values are established for various incremental crack lengths, then the Endure module of NISA can be used to conduct the FCGR analysis, using a variety of FCGR models available within the Endure module (Ref 12). We used the Walker model of Endure, with the parameters established as explained in the previous section, to conduct the FCG. The results of the computational predictions are compared with the experimental results in Fig. 10. The agreement in the results is reasonably good, although there are some differences among the experimental results, and those obtained by the finite element method (FEM) in the region of lower growth rate. For example, $R = 0.1$, the initial growth rate was found to be 2.52×10^{-7} m/cycle experimentally, which is compared to 1.81×10^{-7} and 3.8×10^{-7} m/cycle obtained by the analytical and FEM, respectively (see Fig. 10). On the other hand, the final growth rate was found to be 6.80×10^{-6}, 7.40×10^{-6}, and 6.46×10^{-6} m/cycle, respectfully, obtained experimentally, analytically and numerically, showing much better corroboration.

By examination of the fracture surfaces through SEM images illustrated in Fig. 11, one can see significant serrated and faceted surfaces in the region further away from the initiation zones. These serrated and faceted surfaces indicate that the zone belongs to the propagation zone at the micro level. Moreover, the area hosting these surfaces are larger in the specimens that have been subject to larger stresses, as shown in Fig. 11(b), as opposed to that shown for the lower stress level seen in Fig. 11(a). Larger and more pronounced microcracks were observed in the SEM mages of specimens failed at the higher stress ratio, which can be clearly observed from Fig. 11(c)-(f).

7. Conclusion

Experimental, analytical, and computational investigations were conducted with the aim of characterizing and predicting the fatigue response and crack growth rate of AM60B magnesium alloy at room and elevated temperatures. The influence of the stress ratio was also a primary objective of the investigation.

It is postulated that cracks are initiated in the alloy mainly due to the internal discontinuities due to the presence of porosity, followed by the final fracture resulting from the growth and coalescence of the cracks, as seen in the SEM images.

It was observed that at elevated temperature of 80 °C, the fatigue life of AM60B magnesium alloy decreased. The decrease was not significant at low-stress levels. The initiation of small fatigue cracks generally occurred along the interfaces of the α-Mg grains, due to the micromechanism of the accumulative plastic slipping of surface grains (α-Mg) and the deformation mismatch of the two phases at room temperature. However, the small fatigue cracks mainly cleaved the

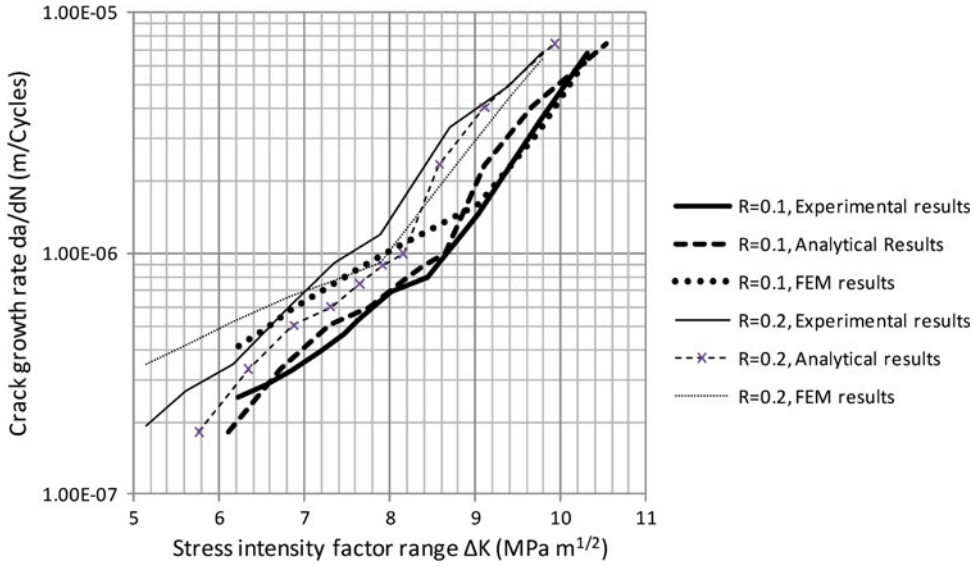

Fig. 10 Comparison of fatigue crack growth rates calculated analytically (Walker model) and those by finite element method

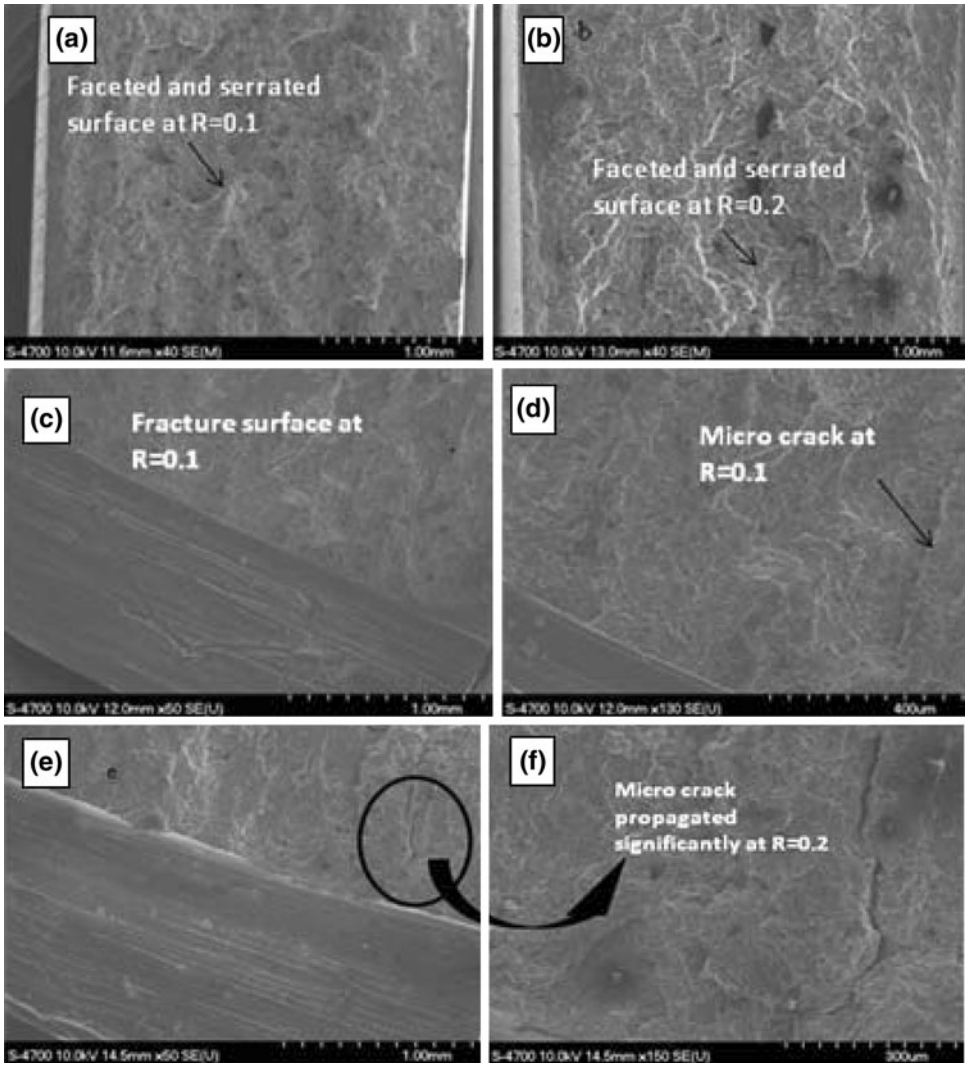

Fig. 11 SEM images showing serrated and faceted surface at (a) $R = 0.1$, (b) $R = 0.2$, (c-f) microcrack found at both stress ratios

α-Mg grains at the elevated temperature. Large segregation of brittle eutectic β-$Mg_{17}Al_{12}$ along the grain boundaries also caused the cleavage of the α-Mg grains at the elevated temperature. At the elevated temperature, the small fatigue cracks propagated through the α-Mg grains, since these regions were softened due to the high temperature.

Walker's model was effectively used for predicting the crack growth rate at various stress ratio of AM60B magnesium alloy based on the data at $R = 0$ baseline. The growth rate was found to increase as stress ratio increased from $R = 0.1$ to 0.2. At $\Delta K = 9.1$ MPa $m^{1/2}$ for stress ratio $R = 0.1$, the growth rate is 1.45×10^{-6} m/cycle. On the other hand, at the same SIF, for $R = 0.2$, the growth rate was found 4.00×10^{-6} m/cycle.

The experimental and analytical results were also very close to those predicted by FE analysis. Further experimental results at higher stresses are required to further establish the concluded trend.

The observed variation in the fatigue crack growth behavior is strongly influenced by the variation in porosity size and distribution within each specimen. Consequently, further studies are needed to clarify the crack propagation behavior at the positive R regions.

Acknowledgments

This research is carried out with the financial support provided by AUT021 Network of Centers of Excellence, an automotive research and development program focusing on issues relating to the automobile in the twenty-first century, as well as the Meridian Technologies. We are indebted to them for the financial support and to IRM (The Institute for Research in Materials, Dalhousie University) for the use of SEM.

References

1. X.S. Wang and J.H. Fan, An Evaluation on the Growth Rate of Small Fatigue Cracks in Cast AM50 Magnesium Alloy at Different Temperatures in Vacuum Conditions, *Int. J. Fatigue*, 2006, **28**, p 79–86
2. N. Grinberg, V. Serdyuk, and I. Ostapenko, Features of Fatigue Failure in Magnesium Alloy MA12 in Air and in Vacuum, *Mech. Mater.*, 1977, **6**, p 61–66
3. R. Stephens, A. Fatemi, R. Stephens, and H. Fuchs, *Metal Fatigue in Engineering*, John Wiley & Sons, Inc., NJ, 1980
4. N. Dowling, *Mechanical Behavior of Materials*, Prentice-Hall Inc., New Jersey, 1998
5. X.S. Wang and J.H. Fan, SEM Online Investigation of Fatigue Crack Initiation and Propagation in Notched cast Magnesium Specimens, *J. Mater. Sci.*, 2004, **39**(7), p 2617–2620
6. T.A. Koch, "Fatigue Properties of High Pressure Die Cast Magnesium AM 60," M.A.Sc. Thesis, Dalhousie University, Department of Metallurgical Engineering, Halifax, NS, Canada, 2004
7. Y. Lu, F. Taheri, and M. Gharghouri, Monotonic and Cyclic Plasticity Responses of High Pressure Die Cast AM60B Magnesium Alloy, *Strain*, 2008 (To Appear)
8. Y. Lu, F. Taheri, and M. Gharghouri, Study of Fatigue Crack Incubation and Propagation Mechanisms in a HPDC AM60B Magnesium Alloy, *J. Alloys Compd.*, 2008, **466**, p 214–227
9. S. Ishihara, A. McEvily, M. Sato, K. Taniguchi, and T. Goshima, The Effect of Load Ratio on Fatigue Life and Crack Propagation Behavior of an Extruded Magnesium Alloy, *Int. J. Fatigue*, 2009, **31**, p 1788–1794
10. R. Zenga, Y. Xub, and E. Hanb, Fatigue Crack Propagation Behavior of an As-Extruded Magnesium Alloy AZ80, *Mater. Sci. Eng. A*, 2009, **509**, p 1–7
11. NISA, *NISA User's Manual, Version 14.0*, Cranes Software Inc., Troy, MI, 2009
12. Endure, *Endure User's Manual, Version 14.0*, Cranes Software Inc., Troy, MI, 1998
13. S. Kleiner, O. Beffort, A. Wahlen, and P. Uggowitzer, Microstructure and Mechanical Properties of Squeeze Cast and Semisolid Cast Mg-Al Alloys, *J. Light Met.*, 2002, **2**, p 277–280
14. ASTM E-8M Standard, "Test Methods of Tension Testing of Metallic Materials [Metric]," *Annual Book of ASTM*, Vol 3(1), American Society of Metals, Metals Park, OH, 2003, p 83–104
15. ASTM E-466 Standard, "Standard Practice for Conducting Force Controlled Constant Amplitude Axial Fatigue Tests of Metallic Materials," *Annual Book of ASTM*, Vol 3(1), American Society of Metals, Metals Park, OH, 2003, p 515−519
16. ASTM E-647 Standard, "Standard Practice for Conducting Force Controlled Constant Amplitude Axial Fatigue Tests of Metallic Materials," *Annual Book of ASTM*, Vol 3(1), American Society of Metals, Metals Park, OH, 1996
17. T.L. Anderson, *Fracture Mechanics: Fundamentals and Applications*, 2nd ed., CRC Press, Inc, FL, 2000, p 573–577
18. A.P. Boresi and R.J. Schmidt, *Advanced Mechanics of Materials*, 6th ed., Wiley, New York, 2002
19. K. Walker, The Effect of Stress Ratio During Crack Propagation and Fatigue for 2024-T3 and 7075-T6 Aluminum, *Effects of Environment and Complex Load Histories on Fatigue Life, ASTM STP 462*, American Society for Testing and Materials, Philadelphia, PA, 1970
20. D. Broek, *The Practical Use of Fracture Mechanics*, FractuREsearch Inc., Galena, OH, 2001, p 44–86
21. T.L. Anderson, *Fracture Mechanics*, 3rd ed., CRC Press Inc., 2005
22. T. Mann, The Influence of Mean Stress on Fatigue Crack Propagation in Aluminum Alloy, *Int. J. Fatigue*, 2007, **29**, p 1393–1401